

# CHAPTER-1

# INTRODUCTION TO ELECTRONIC TRANSPORT IN GRAPHENE SYSTEMS

---

## 1.1 Prologue (Novel Properties of a Novel material)

Could a single piece of a material be the thinnest imaginable material (Single atom thick), the strongest material ‘ever measured’ in terms of Young’s modulus (more than 100 times stronger than the strongest steel), be elastically stiffest known material (stiffer than diamond), be the most stretchable crystal (up to 20% elastically), be almost transparent (absorbs only 2.3% of the light intensity), having record thermal conductivity (outperforming diamond), have highest current density at room  $T$  (106 times of copper), be completely impermeable (even He cannot squeeze through), have highest intrinsic mobility (100 times more than in silicon), show electric current conduction even in the limit of no electrons, having lightest charge carriers (with zero rest mass), have longest mean free path at room temperature (micron range) and possibly possess many more such superlative properties?

Until last decade, even possibility of the existence of a such material namely graphene (or 2D graphite) which possesses all these extra ordinary qualities together was not given proper attention because scientists were puzzled for long time whether nature allows existence of a two dimensional crystal. In 1930’s Peierls [1] and Landau [2] showed that in low-dimensional crystal thermal fluctuations lead to such displacements of atoms that they become comparable to interatomic distances and that would destroy long range order and thus essentially melt 2D lattice at any finite temperature. Hence, graphene has been studied just theoretically for sixty years [3-5]. It was presumed not to exist in the free state, being described as an ‘academic’ material [6] and was believed to be unstable with respect to the formation of curved structures.

Nevertheless, in 2004, a group led by A. K. Geim, from the University of Manchester, UK, isolated such a 2D material [7, 8]. Under the name of graphene, this new material is an allotropic form of carbon and it can be considered the mother of three carbon allotropes (see Figure 1.1), with the atoms arranged in a 2D honeycomb lattice. The reason for the success in synthesis of graphene was the isolation method used by Geim et al. The developed method permitted one to isolate the 2D material on top of a 300-nm-thick wafer of silicon oxide. The weak van-der Waals interaction induced adhesion between graphene and the wafer, and once on top of the wafer, it was possible to move about the 2D material.

Soon after the discovery of graphene several other methods were developed for graphene production, most notably chemical vapor deposition (CVD) [9], segregation by heat treatment of carbon-containing substrates [10] and liquid phase exfoliation [11].

The theory of graphene was first explored by P. R. Wallace [3] in 1947 as a starting point for understanding the electronic properties of 3D graphite. The emergent massless Dirac equation was first pointed out by Gordon Walter Semenoff and David P. DeVincenzo and Eugene J. Mele [12].

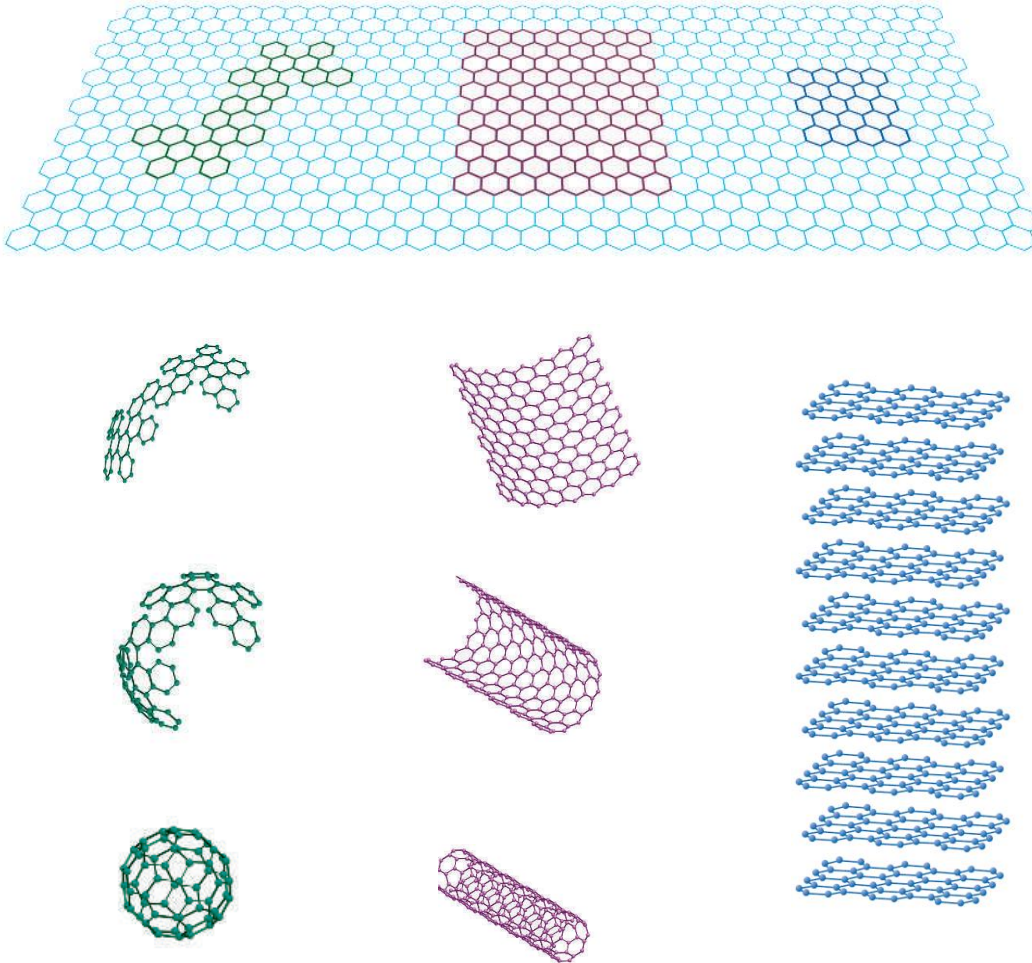


**Figure 1.1:** Graphene can be consider as the mother of three carbon allotropes: (left) byckyballs – zero dimensional structure, (middle) carbon nanotube – one dimensional structure and graphite – three dimensional structure [13].

It has the properties of a good metal, although its electronic properties do not fit the standard theory of metals because its electrons propagate as massless Dirac particles [14]. Graphene is also resistant against extrinsic impurities because its chemical bonding is very specific and consequently graphene conducts electricity better, with less energy loss than silicon [13] (the platform of all modern electronics). Moreover, graphene is one of the strongest materials ever measured in terms of Young's modulus and elastic stiffness [15] (the only other material that is comparable in strength is diamond), nevertheless it is one of softest (the only example of a metallic membrane). It can be used as an ultrasensitive nano-mechanical resonator besides being highly impermeable [16]. Many important properties

have been identified in graphene, including a remarkably high mobility at room temperature, an unusual quantum hall effect, and an ambipolar electric field effect.

## 1.2 Structure and Properties of Monolayer, Bilayer and Monolayer Gapped Graphene

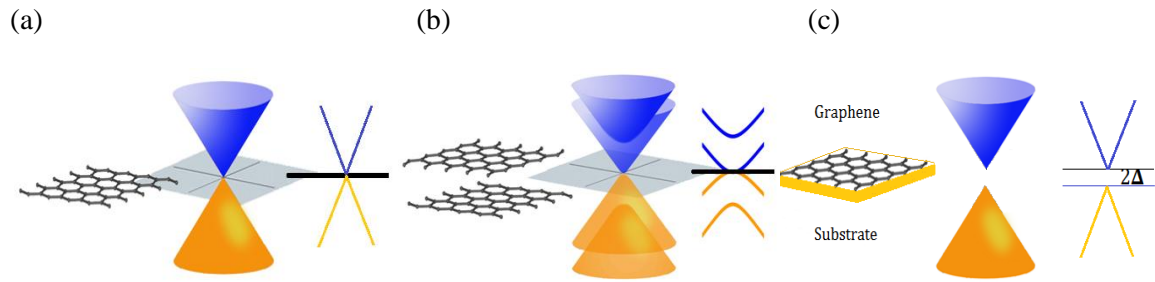


**Figure 1.2:** (a) The electronic structure of monolayer graphene with zero gap, (b) symmetric bilayer graphene with zero gap, and (c) graphene on substrate with gap  $2\Delta$  between valence and conduction band called monolayer gapped graphene.

Monolayer Graphene (MLG) is an isolated single graphite sheet suspended in air having zero energy gap at Dirac point with linear energy dispersion relation, while Bilayer Graphene (BLG) is Bernal Stacking arrangement of two MLG with spacing of nearly  $3.34 \text{ \AA}$  having zero gap at Dirac point with quadratic energy dispersion relation. MLG with finite energy gap at Dirac point with linear energy dispersion relation is called Monolayer Gapped Graphene (MLGG). This gap opening is due to the symmetry breaking of A and B sublattices arising due to interaction between substrate and graphene sheet. In all these graphene based structures, the  $\pi$  electrons are valence electrons which are relevant for the transport and other solid state properties. A tight binding calculation for the  $\pi$  electrons is simple but provides important insights for understanding the electronic structure of the  $\pi$  energy levels or bands for graphene systems. In next sub-sections, band structures and low energy Hamiltonians of MLG, BLG and MLGG using tight binding approximation are discussed briefly.

### 1.2.1 Monolayer Graphene (MLG)

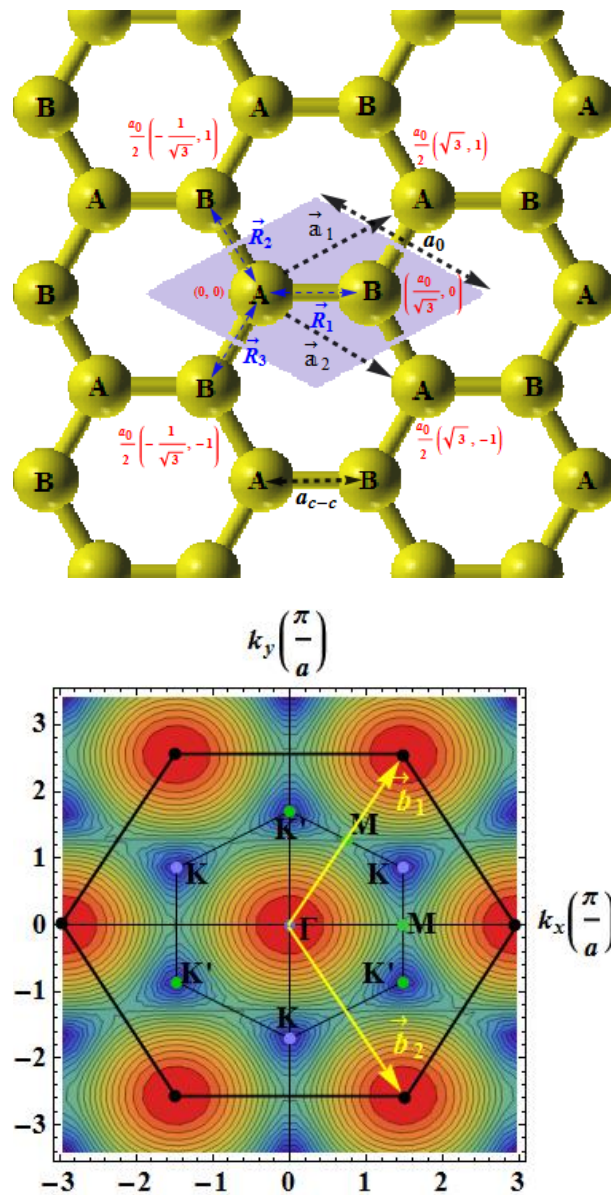


**Figure 1.3:** (a) Honeycomb lattice structure of monolayer graphene and shaded area shows the unit cell of monolayer graphene. (b) Density plot of first Brillouin zone of monolayer Graphene.

Graphene is a two-dimensional material made of carbon atoms arranged in honeycomb lattice with a two-atomic basis (A and B) as seen in Figure 1.3(a). The two primitive lattice vectors of the hexagonal lattice shown in Figure 1.3(a) are

$$\mathbf{a}_1 = \frac{a_0}{2} \begin{pmatrix} \sqrt{3} \\ 1 \end{pmatrix} \text{ and } \mathbf{a}_2 = \frac{a_0}{2} \begin{pmatrix} \sqrt{3} \\ -1 \end{pmatrix}, \quad (1.1)$$

where the lattice constant is  $a_0 = 2.46 \text{ \AA}$  [3]. The Bravais lattice of graphene contain two carbon atoms per unit cell and the area of the unit cell is  $\frac{\sqrt{3}a_0}{4} \approx 5.245 \text{ \AA}^2$ . The primitive reciprocal lattice vectors  $\mathbf{b}_1$  and  $\mathbf{b}_2$  shown in Figure 1.3(b) are

$$\mathbf{b}_1 = \frac{2\pi}{\sqrt{3}a_0} \begin{pmatrix} 1 \\ \sqrt{3} \end{pmatrix} \text{ and } \mathbf{b}_2 = \frac{2\pi}{\sqrt{3}a_0} \begin{pmatrix} 1 \\ -\sqrt{3} \end{pmatrix}. \quad (1.2)$$

There are two inequivalent points  $\mathbf{K}$  and  $\mathbf{K}'$  in the Brillouin zone which are of special interest in Graphene transport physics. Their position in momentum space are given by

$$\mathbf{K} = \frac{2\pi}{\sqrt{3}a_0} \begin{pmatrix} 1 \\ 1/\sqrt{3} \end{pmatrix} \text{ and } \mathbf{K}' = \frac{2\pi}{\sqrt{3}a_0} \begin{pmatrix} 1 \\ -1/\sqrt{3} \end{pmatrix}. \quad (1.3)$$

The vectors connecting three nearest-neighbor in real space are given by

$$\mathbf{R}_1 = \frac{a_0}{2\sqrt{3}} \begin{pmatrix} 2 \\ 0 \end{pmatrix}, \mathbf{R}_2 = \frac{a_0}{2\sqrt{3}} \begin{pmatrix} -1 \\ \sqrt{3} \end{pmatrix} \text{ and } \mathbf{R}_3 = \frac{a_0}{2\sqrt{3}} \begin{pmatrix} -1 \\ -\sqrt{3} \end{pmatrix}. \quad (1.4)$$

Electronic band structure of Graphene is successfully described by tight-binding Hamiltonian model [3]. Graphene is made of carbon with  $sp^2$  hybridization (one's orbital mixed with two p orbitals) and it gives rise to  $\sigma$  bond. While one  $p_z$  orbital remain separate, which is responsible for  $\pi$  bond and therefore tight-binding Hamiltonian calculation involve only the  $p_z$  orbital. In a tight-binding model, the wave function of  $p_z$  orbital is written as

$$|\Psi(\mathbf{r})\rangle = |A\rangle + |B\rangle, \quad (1.5)$$

where

$$|A\rangle = \frac{1}{\sqrt{N}} \sum_{j=1}^N e^{i\mathbf{k}\cdot\mathbf{R}_{A_j}} \left| \varphi_A(\mathbf{r} - \mathbf{R}_{A_j}) \right\rangle \text{ and } |B\rangle = \frac{1}{\sqrt{N}} \sum_{j=1}^N e^{i\mathbf{k}\cdot\mathbf{R}_{B_j}} \left| \varphi_B(\mathbf{r} - \mathbf{R}_{B_j}) \right\rangle. \quad (1.6)$$

Here  $\varphi(\mathbf{r})$  is the wave function of  $p_z$  orbital of a carbon atom located at origin.  $\mathbf{R}_A = n_1\mathbf{a}_1 + n_2\mathbf{a}_2$  and  $\mathbf{R}_B = \mathbf{R}_A + \boldsymbol{\delta}_1$  are the position vectors of all atomic sites for sublattice A and B

respectively where  $n_1, n_2 \in z$ .  $N$  is the number of unit cell and  $\frac{1}{\sqrt{N}}$  ensures normalized wave functions. We consider the only nearest neighbour interaction, tight-binding Hamiltonian in the matrix form is written as

$$H_{\text{TB}}^{\text{MLG}} = \begin{pmatrix} \langle A|\hat{H}|A\rangle & \langle A|\hat{H}|B\rangle \\ \langle B|\hat{H}|A\rangle & \langle B|\hat{H}|B\rangle \end{pmatrix}, \quad (1.7)$$

where, diagonal terms are  $\langle A|\hat{H}|A\rangle = \langle B|\hat{H}|B\rangle = \varepsilon_{2p}$  where  $\varepsilon_{2p}$  is the atomic orbital energy of  $2p_z$  level. The off diagonal terms are defined as

$$\langle A|\hat{H}|B\rangle = -\gamma h(\mathbf{k}), \quad (1.8)$$

where  $\gamma$  is the nearest-neighbour hopping parameter. In Eq. (1.8),  $h(\mathbf{k})$  is defined as

$$h(\mathbf{k}) = \sum_{j=1}^N e^{ik \cdot (\mathbf{R}_j - \mathbf{R}_0)}. \quad (1.9)$$

In the Graphene lattice structure, there are three nearest neighbour atoms as shown in Figure 1.3 (a). So Eq. (1.9) can be written with  $N = 3$ ,

$$h(\mathbf{k}) = e^{ik \cdot \mathbf{R}_1} + e^{ik \cdot \mathbf{R}_2} + e^{ik \cdot \mathbf{R}_3}. \quad (1.10)$$

Read  $\mathbf{R}_1$ ,  $\mathbf{R}_2$  and  $\mathbf{R}_3$  from Eq. (1.4), Eq. (1.10) can be written in more simplified form as

$$h(\mathbf{k}) = \exp\left(ik_x \frac{a_0}{\sqrt{3}}\right) + 2 \exp\left(-ik_x \frac{a_0}{2\sqrt{3}}\right) \cos\left(k_y \frac{a_0}{\sqrt{3}}\right). \quad (1.11)$$

From Eq. (1.7), Hamiltonian matrix becomes

$$H_{\text{TB}}^{\text{MLG}} = \begin{pmatrix} \varepsilon_{2p} & \gamma h(\mathbf{k}) \\ \gamma h^*(\mathbf{k}) & \varepsilon_{2p} \end{pmatrix}. \quad (1.12)$$

We also define the overlap matrix as,

$$S = \begin{pmatrix} \langle A|A\rangle & \langle A|B\rangle \\ \langle B|A\rangle & \langle B|B\rangle \end{pmatrix}. \quad (1.13)$$

The diagonal elements are  $\langle A|A \rangle = \langle B|B \rangle = 1$  and off diagonal elements are defined in a same manner as the Hamiltonian matrix

$$\langle A|B \rangle = s h(\mathbf{k}), \quad (1.14)$$

where,  $s$  is the overlap integral and its value is 0.129 eV. Then overlap matrix can be written as

$$S = \begin{pmatrix} 1 & s h(\mathbf{k}) \\ s h^*(\mathbf{k}) & 1 \end{pmatrix}. \quad (1.15)$$

The eigenvalue equation can be calculated by  $\det (H-ES) = 0$ ;

$$\begin{vmatrix} \varepsilon_{2p} - E & -\gamma h(\mathbf{k}) - E s h(\mathbf{k}) \\ -\gamma h^*(\mathbf{k}) - E s h^*(\mathbf{k}) & \varepsilon_{2p} - E \end{vmatrix} = 0. \quad (1.16)$$

This simplifies that

$$E^2 - s |h(\mathbf{k})|^2 (-\gamma - s E)^2 = 0. \quad (1.17)$$

The energy dispersion relation as a function of  $h(\mathbf{k})$  is then given by

$$E_{v(c)}(\mathbf{k}) = \frac{\varepsilon_{2p} - (+)\gamma |h(\mathbf{k})|}{1 + (-)s |h(\mathbf{k})|}, \quad (1.18)$$

where the + and - signs in the Eq. (1.18) for conduction band and valance band respectively.

The function  $|h(\mathbf{k})|$  is given by:

$$|h(\mathbf{k})| = \sqrt{1 + 4 \cos^2 \left( k_y \frac{a_0}{\sqrt{3}} \right) + 4 \exp \left( -i k_x \frac{a_0}{2\sqrt{3}} \right) \cos \left( k_y \frac{a_0}{\sqrt{3}} \right)}. \quad (1.19)$$

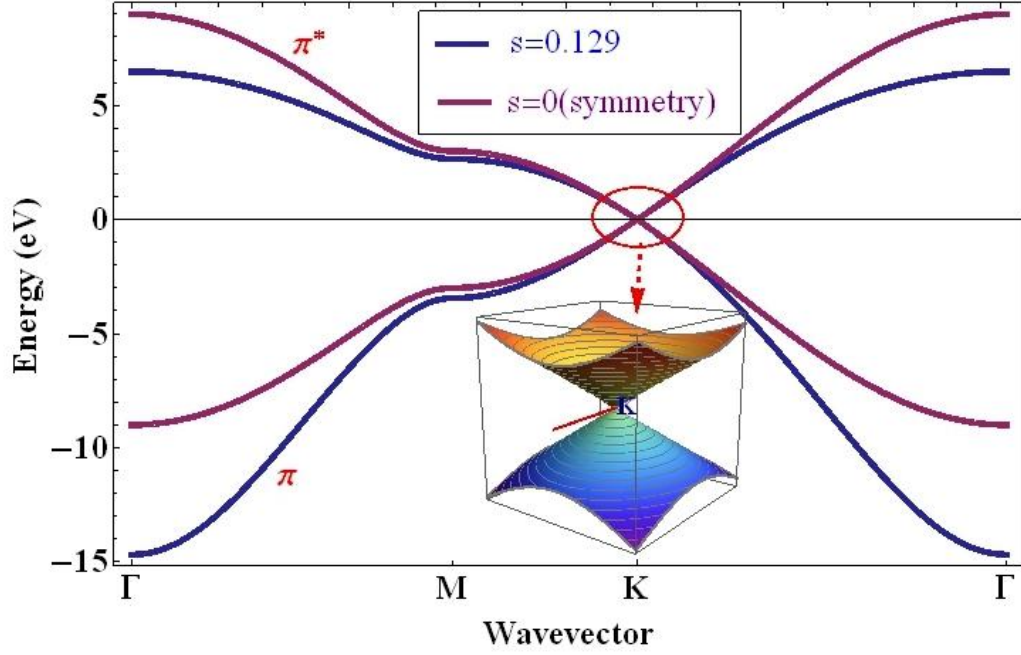


**Figure 1.4:** The  $\pi$  band structure of Graphene plotted using nearest-neighbour tight-binding model along  $\Gamma \rightarrow M \rightarrow K \rightarrow \Gamma$ . The Fermi level lies at the centre  $E = 0$ .

To calculate the  $\pi$  band structure of Graphene from Eq. (1.18), three parameters  $\varepsilon_{2p}$ ,  $\gamma$  and  $s$  should be known and their values are found by fitting experiment or ab-initio calculation. Past calculation show  $\varepsilon_{2p}$  is set to zero,  $\gamma$  vary between 2.5 eV to 3 eV and  $s \approx 0.129$ . One can simplify Eq. (1.18) by setting  $\varepsilon_{2p} = 0$  (its means Fermi energy is set to zero) and  $s = 0$  for electron-hole symmetry arguments, then we arrive at

$$E_{v(c)}(\mathbf{k}) = -(+)\gamma \sqrt{1 + 4 \cos^2 \left( k_y \frac{a_0}{\sqrt{3}} \right) + 4 \exp \left( -ik_x \frac{a_0}{2\sqrt{3}} \right) \cos \left( k_y \frac{a_0}{\sqrt{3}} \right)}. \quad (1.20)$$

Asymmetric ( $s = 0.129$ ) and symmetric ( $s = 0$ ) electronic band structure calculated using Eqs. (1.18) and (1.20) respectively are plotted in Figure 1.4 for inserting  $\gamma = 3$  eV. The upper half of the dispersion is the conduction band ( $\pi^*$ ) and the lower half dispersion is valance band ( $\pi$ ). In Figure 1.4, electronic band structure calculated at two different values of  $s(= 0.129 \& 0)$  are seems to be same and approximately linear at low energy regime (as shown in inset). Graphene band structure shows that zero band gap i.e. semimetal at Fermi

energy and conduction and valance band touch to each other at  $\mathbf{K}$  point. Then there are two lines that are linear around the  $\mathbf{K}$  point ( $\mathbf{k}, \mathbf{p}$  approximation or linear expansion). Thus for small values of  $\mathbf{k}$  (i.e. with respect to the  $\mathbf{K}$  point), the energy dispersion can be approximated by a linear dispersion relation. This dispersion near to Dirac points can be obtained by expanding Eq. (1.11) close to the  $\mathbf{K}$  (or  $\mathbf{K}'$ ) vector, Eq. (1.3), as  $\mathbf{k} = \mathbf{K} + \mathbf{q}$ :

$$h(\mathbf{K} + \mathbf{q}) = \sum_{j=1}^N e^{i(\mathbf{K}+\mathbf{q})\cdot\mathbf{R}_j}. \quad (1.21)$$

For  $\mathbf{K} \gg \mathbf{q}$ , Eq. (1.21) can be approximate as a

$$h(\mathbf{K} + \mathbf{q}) = i \sum_{j=1}^N e^{i\mathbf{K}\cdot\mathbf{R}_j} \mathbf{q} \cdot \mathbf{R}_j = ie^{i\mathbf{K}\cdot\mathbf{R}_1} \mathbf{q} \cdot \mathbf{R}_1 + ie^{i\mathbf{K}\cdot\mathbf{R}_2} \mathbf{q} \cdot \mathbf{R}_2 + ie^{i\mathbf{K}\cdot\mathbf{R}_3} \mathbf{q} \cdot \mathbf{R}_3. \quad (1.22)$$

We insert the values of  $\mathbf{R}_j$  from Eq. (1.4) into the above equation and we get final result;

$$h(\mathbf{K} + \mathbf{q}) \approx \frac{\sqrt{3}a_0}{2} \left( \frac{\sqrt{3}}{2} + i \frac{1}{2} \right) (-q_x + iq_y) = -\frac{\sqrt{3}a_0}{2} e^{i\pi/6} (q_x - iq_y). \quad (1.23)$$

From Eq. (1.12), Hamiltonian matrix near to Dirac points is written as,

$$H_{\text{TB}}^{\text{MLG}} = -\frac{\sqrt{3}a_0\gamma}{2} \begin{pmatrix} 0 & e^{i\pi/6}(q_x - iq_y) \\ e^{-i\pi/6}(q_x + iq_y) & 0 \end{pmatrix}. \quad (1.24)$$

In the calculation of energy eigenvalue equation, we can ignore phases  $e^{\pm i\pi/6}$  because they cancel out each other.

$$H_{\text{TB}}^{\text{MLG}} = \hbar v_f \begin{pmatrix} 0 & (q_x - iq_y) \\ (q_x + iq_y) & 0 \end{pmatrix}, \quad (1.25)$$

where  $v_f = \frac{\sqrt{3}a_0\gamma}{2\hbar} \approx 10^6 \text{m/s}$  is the Fermi velocity which is 300 times smaller than light velocity. The eigenvalues are then simply define as

$$E_{v(c)}(\mathbf{k}) = -(+)\hbar v_f |\mathbf{q}|, \quad (1.26)$$

where  $|\mathbf{q}| = \sqrt{q_x^2 + q_y^2}$ . This Dirac like linear behaviour valid up to  $\sim 1 \text{ eV}$ , as seen from the band structure in Fig. 2.

## 1.2.2 Bilayer Graphene (BLG)

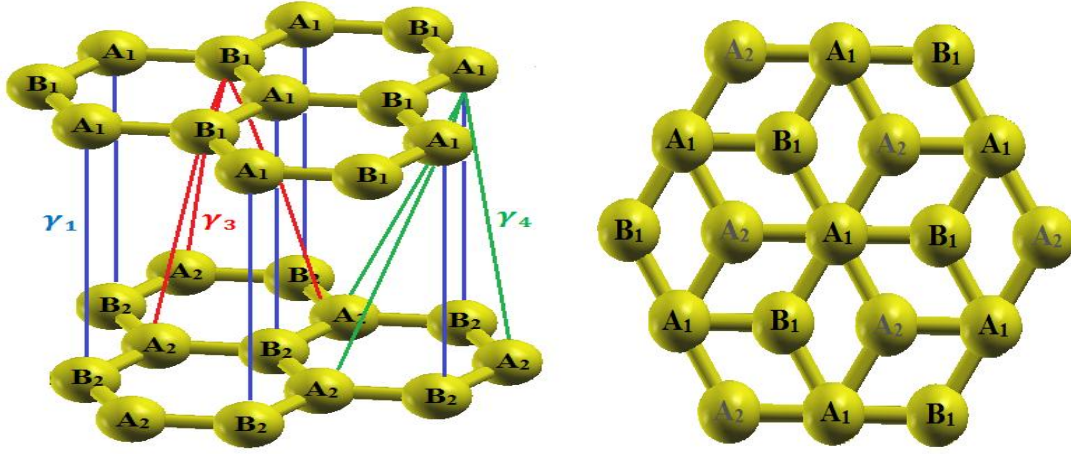


**Figure 1.5:** The lattice structure of a bilayer Graphene. Some representative hopping integrals are shown. (a) Conventional Graphene with AB stacking and (b) top view of bilayer graphene.

Bilayer Graphene is the natural graphite with considering only two layers which are arranged in the  $A_1B_2$  (Bernal) stacking as shown in Figure 1.5. The top layer is denoted as 1 and the bottom layer denoted as 2. In each layer, the unit cell contains two carbon atoms denoted by  $A_1$  and  $B_1$  in layer 1 and  $A_2$  and  $B_2$  in layer 2. Carbon atoms  $A_1$  of layer 1 lie directly above the carbon atoms  $B_2$  of layer 2, while the carbon atoms  $B_1(A_2)$  of layer 1 (layer 2) lie over the centre of hexagonal cell of layer 2 (layer 1) [17]. In Figure 1.5,  $\gamma_1 \approx 0.39$  eV is interlayer coupling between sites  $A_1$  and  $B_2$ ,  $\gamma_3 = 0.315$  eV is interlayer coupling between sites  $B_1$  and  $A_2$  and  $\gamma_4 \approx 0.04$  eV is interlayer coupling between sites  $A_1$  and  $A_2$  and  $B_1$  and  $B_2$ . The Hamiltonian matrix and energy dispersion relation for bilayer Graphene can be easily derived from the same methods as described in above section (1.2.1). We consider only the interlayer coupling between vertically neighbouring atoms, then Hamiltonian for bilayer Graphene is [17]

$$H = \begin{pmatrix} 0 & \gamma h(\mathbf{k}) & 0 & 0 \\ \gamma h^*(\mathbf{k}) & 0 & \gamma_1 & 0 \\ 0 & \gamma_1 & 0 & \gamma h(\mathbf{k}) \\ 0 & 0 & \gamma h^*(\mathbf{k}) & 0 \end{pmatrix} \quad (1.27)$$

and energy dispersion relation is calculated from Eq. (1.17) is

$$E_{v(c)}^{\text{BLG}}(\mathbf{k}) = -(\pm)\frac{\gamma_1}{2} - (\pm)\frac{1}{2}\sqrt{\gamma_1^2 + 4\gamma^4|h(\mathbf{k})|^4}. \quad (1.28)$$

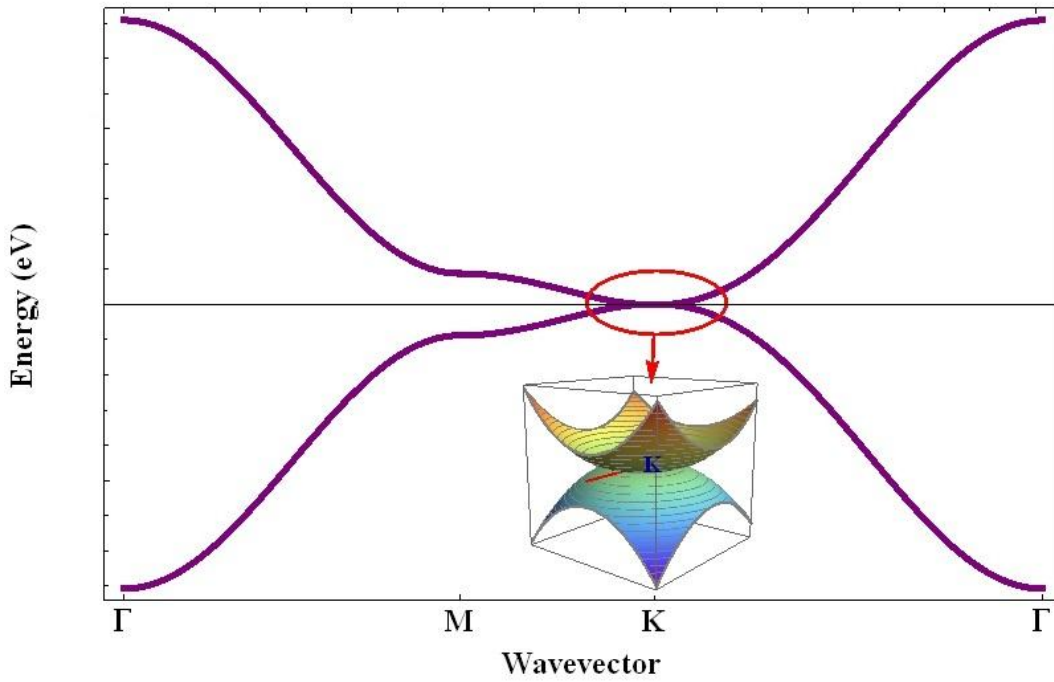


**Figure 1.6:** The  $\pi$  band structure of bilayer Graphene plotted using nearest-neighbor tight-binding model along  $\Gamma \rightarrow M \rightarrow K \rightarrow \Gamma$ . The Fermi level lies at the center  $E = 0$ .

As can be seen from Figure 1.6, bilayer Graphene has a zero-gap structure at the K points, but with quadratic dispersion unlike monolayer. One more interesting point of bilayer Graphene is it has nonzero density of states even at zero energy [18] unlike monolayer Graphene where density of state vanishes at zero energy. In the vicinity of  $E = 0$ , the Hamiltonian in Eq. (1.27) is reduced to the  $2 \times 2$  form for the basis set  $(A1, B2)$  and corresponding energy dispersion relation become  $E_{v(c)}^{\text{BLG}}(\mathbf{k}) = -(\pm)\hbar^2|\mathbf{k}|^2/(2m)$  [17].

### 1.2.3 Monolayer Gapped Graphene (MLGG)

In the previous section (1.2.1) we saw that Graphene is zero bandgap with its valance and conduction bands touching at Dirac points. The absence of band gap makes it challenging for Graphene to be used in device applications. Recently, some experiments based on angle-resolved photoemission spectroscopy (ARPES) have shown the opening of band gap of 260 meV & 53 meV on Graphene sample epitaxially grown on SiC (Silicon Carbide) & BN (Boron Nitride) substrates, respectively. This gap opening is due to the symmetry breaking of A and B sublattices arising due to interaction between substrate and Graphene sheet [19-22]. Theoretically, it is possible to introduce a band gap of exactly  $E_g = 2\Delta$  by shifting the on-site energies at two sublattices (A & B) in Monolayer Graphene (MLG) is called Monolayer Gapped Graphene (MLGG). The Hamiltonian matrix of MLGG is simply modify by  $\varepsilon_{2p} = \pm \Delta$  in MLG's Hamiltonian Eq. (1.17);

$$\begin{vmatrix} \Delta - E & -\gamma h(\mathbf{k}) - E s h(\mathbf{k}) \\ -\gamma h^*(\mathbf{k}) - E s h^*(\mathbf{k}) & -\Delta - E \end{vmatrix} = 0. \quad (1.29)$$

This simplifies that

$$-(\Delta^2 - E^2) - |h(\mathbf{k})|^2(\gamma + s E)^2 = 0. \quad (1.30)$$

Eq. (1.30) is a quadratic equation in E with the solutions

$$E_{v(c)}(\mathbf{k}) = \frac{-\gamma s |h(\mathbf{k})|^2 - (+)\sqrt{\Delta^2 + |h(\mathbf{k})|^2 (\gamma^2 - s^2 \Delta^2)}}{1 - s^2 |h(\mathbf{k})|^2}. \quad (1.31)$$

I further simplify Eq. (1.31) for symmetric electronic band structure where  $s = 0$  keep in above Eq. (1.31),

$$E_{v(c)}(\mathbf{k}) = -(+)\sqrt{\Delta^2 + \gamma^2 |h(\mathbf{k})|^2}, \quad (1.32)$$

where  $|h(\mathbf{k})|$  is define in Eq. (1.19). In Dirac approximation as discussed in section (1.2.1),  $|h(\mathbf{k})| \approx \hbar v_f |\mathbf{k}|$  around the K points in Brillouin zone and the energy become

$$E_{v(c)}(\mathbf{k}) = -(+)\sqrt{(\hbar v_f |\mathbf{k}|)^2 + \Delta^2}. \quad (1.33)$$

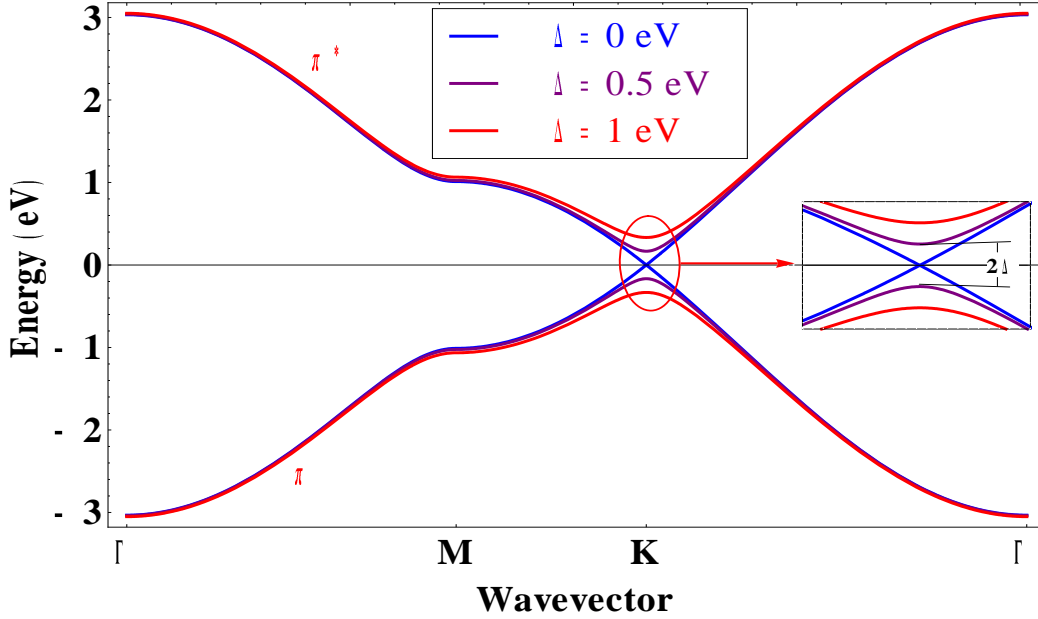


**Figure 1.7:** The  $\pi$  band structure of graphene plotted for different values of gap using nearest-neighbor tight-binding model along  $\Gamma \rightarrow M \rightarrow K \rightarrow \Gamma$ . The Fermi level lies at the center  $E = 0$ . Here we used  $s = 0$  for symmetric band structure.

The band structure of gapped graphene is shown in Figure 1.7 for different values of  $\Delta$ , calculated using Eq. (1.32). It is clear that gap open at the K point for finite value of  $\Delta$  and bands separate more and more as  $\Delta$  increases.

### 1.3 Electronic Transport in Graphene Systems

In this section, I present brief introduction to methods which are used to find transport properties of Graphene. Specifically I have adopted an approach of first calculating screened coulomb potential using random phase approximation (RPA) and then using this screened coulomb potential to calculate electron impurity scattering rate in Graphene using Boltzmann

transport theory. There are other alternate methods/approximations for transport scattering mechanisms of Graphene like; Self Consistent Born Approximation (SCBA) for short-range scatterers at Dirac point; Landauer's approach for pristine Graphene ribbon in ballistic regime, Effective Medium Theory (EMT) for nonlinear screening in Graphene. I have also discussed recent works on transport properties of Graphene systems.

### 1.3.1 Screening

Coulomb interaction plays a key role in most branches of physics. A major feature of this interaction is its long range, varying as  $1/r$  with the distance of the interacting particles. Therefore, a collection of carriers in a material is likely to strongly interact and a charge fluctuation at any one point has non-negligible effects at large distances. In reality however, the electrical attraction or repulsion between charge particles are suppressed for long-range and reduces the effective interaction between charge particles. This reduction of charge particles interaction, and the weakening of internal electric field, is usually referred to as "screening". In Graphene, unlike normal metals, charge carriers and impurities are highly screened by the Fermi sea. The introduction of charges to a neutral Graphene sheet has several competing effects on its transport properties, due to the screening of the electron-electron interaction and the screening of long-range impurities. The effect of electronic screening in Graphene has been extensively studied in the past at zero temperature [23-29] as well as at finite temperature [30-33]. Two widely prevalent theories [34, 35] are used to calculate screening induced by the mobile charge in Graphene:

- (a) Thomas–Fermi Approximation (TFA)
- (b) Random Phase Approximation (RPA)

## (a) Thomas–Fermi Approximation (TFA)

Thomas–Fermi (TF) screening adopts a semi-classical approximation that requires the screened potential to vary slowly. This approximation is valid even when a linear relation between induced charge density ( $\rho^{ind}$ ) and total potential ( $\phi$ ) does not hold and it violets in the limit of  $r \rightarrow 0$  (or, equivalently, large  $q$ ). The screened coulomb interaction in TFA for Graphene is given by

$$V_{sc}^{TF}(q) = v_q / \epsilon_{TF}(q), \quad (1.34)$$

where  $v_q = 2\pi e^2 / (\kappa q)$  is bare coulomb potential and  $\epsilon_{TF}(q)$  is the static dielectric function in TFA it is given by;  $\epsilon_{TF}(q) = \left(1 + \frac{\pi}{2} \frac{\alpha}{4}\right)$  [36] and  $\epsilon_{TF}(q) = \left(1 + \frac{q_{TF}}{q}\right)$  [30] for undoped and doped Graphene, respectively. Here,  $q_{TF} = 4e^2 k_f / (\kappa \gamma)$  is TFA wave vector in doped Graphene and  $\alpha = 4e^2 / (\kappa \gamma)$  is dimensionless coupling constant (it is defined as  $r_s = e^2 / \kappa \gamma$  i.e. a ratio of the Coulomb to kinetic energy and we will use  $\alpha = 4r_s$ ) of graphene which depends only on material parameters and is independent of electron doping. Dielectric function  $\epsilon_{TF}(q)$  of doped graphene in TFA (also in RPA) become infinity in long wavelength limit ( $q \rightarrow 0$ ) and it behaves as a metallic like screening where charge is free to move and the medium is therefore infinitely polarizable due to finite density of state at Fermi level enables intraband transitions. However dielectric function is constant in the case of undoped graphene where it shows the dielectric like screening due to vanishing density of state at Fermi level and enables intraband transitions. The TFA wavevector ( $q_{TF}$ ) is dependent of energy (or density of state) and consequently  $q_{TF} \sim k_f \sim \sqrt{n_c}$ , where  $n_c$  is carrier concentration. However, it is independent of the energy (or density of state) in bilayer graphene and 2-Dimensional Electron Gas. A key dimensionless quantity determining the charged impurity scattering limited transport in electronic materials is  $q_s = q_{TF} / k_f$  which controls the dimensionless strength of quantum screening. In MLG,  $q_s$  being a constant

implies that the screened Coulomb interaction has exactly the same behavior as the unscreened bare Coulomb interaction. In BLG and 2DEG,  $q_s = q_{TF}/k_f \sim 1/\sqrt{n_c}$  and effective screening increases as the carrier density decreases ( $n_c$ ). Hence close to Dirac point, where  $n_c = 0$ ,  $q_s \rightarrow \infty$  and the interaction term should dominate the kinetic term. Therefore screening is more profound in BLG than in MLG.

The TFA model is valid for the system weakly perturbed by a small distribution of external charges and do not require frequency- dependent dielectric function i.e.  $\epsilon(q)$ . But it fails when the screening of the interaction between the rapidly moving charges in a system and it is necessary to develop a formulation capable of describing the screening of a longitudinal field which varies in both space and time i.e.  $\epsilon(q, \omega)$ . This deficiency may be overcome by using random phase approximation (RPA) where dielectric function model as a weak time-dependent perturbation depending on both space and time.

### **(b) Random Phase Approximation (RPA)**

In RPA, one exploits the approximation that the induced charge density contributes linearly to the total potential. The Schrödinger equation is then used to calculate the electronic wave functions self-consistently in the presence of the new potential. In this approximation it is assumed that only the single-particle excitations of the same wave vector as the Coulomb interaction plays an effective role in the screening process while the effects of others having different wave vectors cancel out. Use of the RPA is justified when the electron-electron interaction is strong enough ( $r_s \ll 1$ ) that quantum coherence does not dominate. Monolayer Graphene is a weakly interacting system since the coupling constant ( $r_s \leq 2$ ) is never large [37] and RPA is the most successful and widely accepted approaches in Graphene systems. In high density electron gas, nearly full contribution comes from the ‘ring’ diagrams (Random Phase Approximation). The resulting screened Coulomb interaction

is thus given by the bare Coulomb interaction dressed by a series of bubble diagrams, as shown in Figure 1.8.

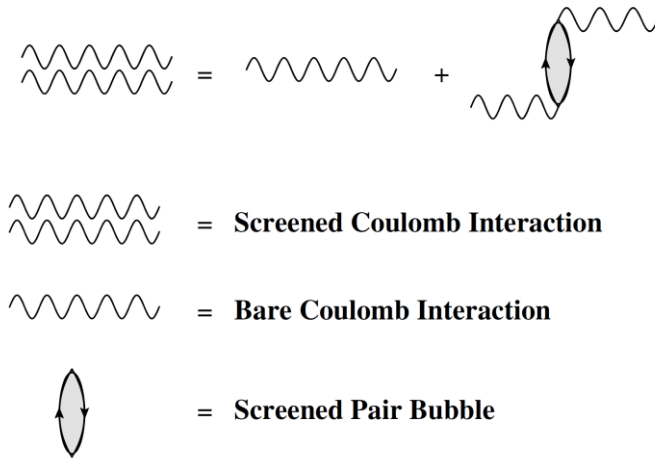


**Figure 1.8:** The Feynman diagram for the screened Coulomb interaction within the RPA. The double and single wiggly lines denote respectively the RPA screened and bare interaction, and shaded ring diagram show the polarization part.

The double wiggly line is known as screened coulomb interaction  $V_{sc}^{RPA}(q, \omega)$  in RPA, while the single wiggle is bare coulomb interaction  $v_q$ . In this diagram pair bubble diagram show the polarization part. The expression of screened coulomb interaction can be read directly from above diagram (or from Figure 1.8):

$$V_{sc}^{RPA}(q, \omega) = v_q + \Pi_{RPA}(q, \omega). \tag{1.35}$$

$\Pi_{RPA}(q, \omega)$  is the polarization function in RPA and it show how the interaction causes the medium to become “virtually polarized” in all possible ways. Graphical representation of  $\Pi_{RPA}(q, \omega)$  is shown in Figure 1.9.

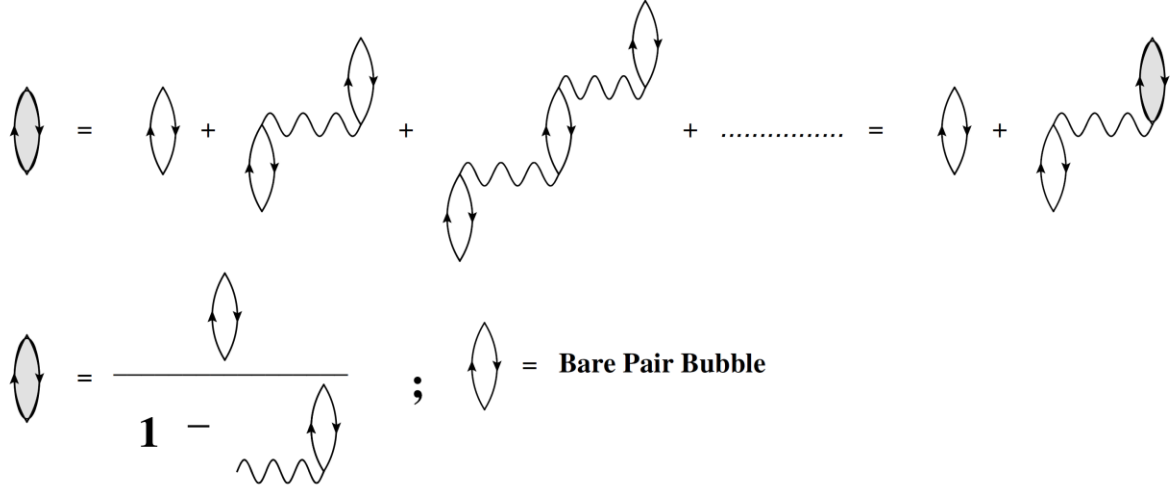


**Figure 1.9:** The Feynman diagram for the polarizability (dressed bubble diagram) for interaction electron system in RPA. The bare bubble diagram is corresponding non interacting electron contribution.

The expression of  $\Pi_{\text{RPA}}(\mathbf{q}, \omega)$  can be read directly from above diagram (or from Figure 1.9):

$$\Pi_{\text{RPA}}(\mathbf{q}, \omega) = \frac{\Pi_0(\mathbf{q}, \omega)}{1 - v_q + \Pi_0(\mathbf{q}, \omega)}. \quad (1.36)$$

The dressed bubble is also known as the polarizability of the interacting electron gas, while the bare bubble is the polarizability of the noninteracting electron gas. The nomenclature results from observing that a pair bubble represents a virtual process (energy is not conserved) in which an electron–hole pair is created and then annihilated. An electron in state below the Fermi surface absorbs momentum  $q$  and moves above the Fermi surface; its absence from the Fermi sphere is equivalent to the presence of a hole. The electron then surrenders the momentum  $q$ , and recombines with the hole. The electron and the hole, being of opposite charges, their creation is tantamount to the creation of a dipole moment, which causes the medium to become polarized. The bare pair bubble is given by

$$\Pi_0(\mathbf{q}, \omega) = \frac{g}{V} \sum_{\mathbf{k}} \frac{f_{\mathbf{k}} - f_{\mathbf{k}+\mathbf{q}}}{\varepsilon_{\mathbf{k}} - \varepsilon_{\mathbf{k}+\mathbf{q}} + i\hbar\omega}. \quad (1.37)$$

We can also write screened coulomb potential in form of  $\Pi_0(\mathbf{q}, \omega)$  using Eq. (1.35) and Eq. (1.36)

$$V_{sc}^{RPA}(\mathbf{q}, \omega) = \frac{v_q}{1 - v_q \Pi_0(\mathbf{q}, \omega)} \quad (1.38)$$

In Eq. (1.38), denominator terms define as;

$$\epsilon_{RPA}(\mathbf{q}, \omega) = 1 - v_q \Pi_0(\mathbf{q}, \omega) = 1 - \frac{g}{V} \sum_k \frac{f_k - f_{k+q}}{\epsilon_k - \epsilon_{k+q} + i\hbar\omega}, \quad (1.39)$$

where  $\epsilon_{RPA}(\mathbf{q}, \omega)$  is the dielectric function, which measures the response of the interacting electron gas to an external electric potential. The dielectric function is the central quantity to theoretical understanding of various many-body aspect such as; screening of the potential due to charged particle (i.e.  $V_{sc}(\mathbf{q}, \omega) = v_q / \epsilon(\mathbf{q}, \omega)$ ), optical properties, collective excitations (i.e.  $\text{Re}[\epsilon(\mathbf{q}, \omega)] = 0$ ), exchange and correlation energy, self-energy, static structure factor, pair-correlation function, local field correction, density of screened charge etc.

### 1.3.2 Boltzmann Transport Equation

Recent past experiments on conductivity of Graphene away from the Dirac point showed that the conductivity in graphene increases linearly with carrier density concentration. Theoretically this linear carrier density dependence of experimental conductivity is successfully explained through the Boltzmann Transport theory at high carrier density limit. The Boltzmann transport equation is powerful technique that governs electronic motion affected by external electric field, scattering due to impurities, phonons and even other electrons in the system. In Boltzmann Transport theory, we start by assuming the system to be a homogeneous 2D carrier system of electrons (or holes) with a carrier density induced by the external gate voltage  $V_g$  and collision is elastic therefore we can neglect interband processes ( $s' \neq s$ ). When the external electric field is weak and the displacement of

the distribution function from thermal equilibrium is small, we may write the distribution function to the lowest order in the applied electric field ( $\mathbf{E}$ ), we have

$$f_{sk}^E = f(E_{sk}) + g_{sk}, \quad (1.40)$$

where  $f(E_{sk})$  is the Fermi distribution function and  $g_{sk}$  is the deviation proportional to  $\mathbf{E}$ .

Then, we have

$$\frac{dk}{dt} \frac{\partial f_{sk}^E}{\partial k} = -e \mathbf{E} \cdot \vartheta_{sk} \frac{\partial f}{\partial E_{sk}} - \frac{e}{c \hbar} (\vartheta_{sk} \times \mathbf{B}) \cdot \frac{\partial g_{sk}}{\partial k}, \quad (1.41)$$

Where  $\mathbf{B}$  is the magnetic field perpendicular to the system and  $\vartheta_{sk}$  is the velocity given by

$$\vartheta_{sk} = \frac{\partial E_{sk}}{\hbar \partial k} = \frac{\gamma}{\hbar} \frac{sk}{|k|}. \quad (1.42)$$

The vector product is define as  $\vartheta_{sk} \times \mathbf{B} = -\mathbf{B} \times \vartheta_{sk} = \mathbf{B}(\vartheta_y - \vartheta_x)$  for vector  $\vartheta_{sk} = (\vartheta_x, \vartheta_y)$ . In the Boltzmann transport equation, the rate of change of the distribution function  $f_{sk}^E$  due to elastic scattering is given by

$$\frac{dk}{dt} \frac{\partial f_{sk}^E}{\partial k} = - \sum_{s'} \int \frac{dk'}{(2\pi)^2} [f_{sk}^E (1 - f_{s'k'}^E) - f_{s'k'}^E (1 - f_{sk}^E)] W(s'k', sk), \quad (1.43)$$

where  $W(s'k', sk)$  is the transition probability. The transition probability from state  $k$  to state  $k'$  is given by Fermi golden's rule:

$$W(s'k', sk) = \frac{2\pi}{\hbar} \langle |V_{s'k',sk}|^2 \rangle \delta(E_{sk} - E_{s'k'}), \quad (1.44)$$

where  $V_{s'k',sk}$  is the matrix element of scattering potential and  $\langle \dots \rangle$  denotes the average over configurations of scatterers. In Eq. (1.44),  $\delta(E_{sk} - E_{s'k'})$  function ensuring energy conservation. From Eqs. (1.41) and (1.43), the transport equation is rewritten as

$$e \mathbf{E} \cdot \vartheta_{sk} \left( -\frac{\partial f}{\partial \varepsilon_{sk}} \right) = \frac{e}{c \hbar} (\vartheta_{sk} \times \mathbf{B}) \cdot \frac{\partial \mathbf{g}_{sk}}{\partial k} - \int \frac{dk'}{(2\pi)^2} (\mathbf{g}_{sk} - \mathbf{g}_{s'k'}) \frac{2\pi}{\hbar} \langle |V_{s'k',sk}|^2 \rangle \delta(E_{sk} - E_{s'k'}). \quad (1.45)$$

The second term on the right hand side of Eq. (1.45) accounts for the relaxation time;

$$\frac{\hbar}{\tau(\varepsilon_{sk})} = 2\pi \int \frac{dk'}{(2\pi)^2} [1 - \cos(\theta_k - \theta_{k'})] \frac{2\pi}{\hbar} \langle |V_{s'k',sk}|^2 \rangle \delta(E_{sk} - E_{s'k'}). \quad (1.46)$$

The factor  $[1 - \cos(\theta_k - \theta_{k'})]$  favors large-angle scattering. The term  $\langle |V_{s'k',sk}|^2 \rangle$  can be replaced by  $n_i |V(q)/\varepsilon(q)|^2 F_{ss'}(k, k')$  where  $n_i$  is the impurity density,  $V(q)$  the Fourier transform of the scattering potential, and  $F_{ss'}(k, k')$  is the chiral function.  $\varepsilon(q)$  is the static dielectric function as discussed in previous section.

### 1.3.3 Recent Works on Transport Properties of Graphene Systems

The nature of electronic transport in graphene has been actively debated over the last decade, and the nature of the graphene Dirac point has been elucidated (make clear/ explain) through experimental and theoretical works studying density and temperature-dependent electrical conductivity [13, 14, 38, 39]. In undoped graphene, conductivity calculated at the Dirac point should be zero due to vanishing density of states. However, many experimental groups using different approaches show a finite conductivity or minimum conductivity  $\sigma_{min} = 4e^2/h$  at zero energy (or  $V_g = 0$ ) which is independent of the impurity concentration, even if the concentration of impurities is a small number [8, 40-42]. Moreover this kind of minimum conductivity near the Dirac point were also probed experimentally in BLG [42-45]. The existence of a conductivity minimum ( $\sigma_{min}$ ) in both MLG and BLG is also referred to as quantum-limited resistivity [46]. Recent experimental results [41, 48, 49] provide convincing evidence that  $\sigma_{min}$  at the Dirac point is due to the random charged impurities located in the graphene environment and that are the dominant source of disorder

in graphene. Theoretically this  $\sigma_{min}$  of graphene at Dirac point have been achieved in different approximation, such as Self-Consistent Born Approximation (SCBA) [18, 50-52], Effective Medium Theory (EMT) with nonlinear screening effects [53, 54], Kubo formula based on linear response theory [55-57], Landauer formula for a rectangular graphene system with aspect ratio  $W/L \ll 1$  [58-60]. Theoretically predicted minimum conductivity in MLG is smaller than that of the experimentally observed.

In SCBA, for simplicity, electrons in MLG and BLG scatters from the short range scatterers with delta like potential. The  $\sigma_{min}$  exhibits  $4e^2/(\pi h)$  for MLG and  $8e^2/(\pi h)$  for BLG [51] with neglecting trigonal warping which is twice the value in MLG. Similar result also found by J. Cserti [57] using the Kubo formula. In the presence of trigonal warping, the  $\sigma_{min}$  for BLG leads to  $24e^2/(\pi h)$  [51] because of multiple Fermi surface pockets at low energies.

K. Nomura and A. H. MacDonald [56] argued that  $\sigma_{min}$  could be enhanced from  $\sigma_{min} = e^2/(\pi h)$  for short range scatterers to  $\sigma_{min} = 4e^2/(\pi h)$  for Coulomb scatterers. Later based on linear response theory (Kubo formula) [55], the ballistic transport leads to  $\sigma_{min} = \pi e^2/h$  for the pure graphene system and this  $\sigma_{min}$  does not depend on the strength of impurity scattering because the change of the diffusion coefficient is completely compensated by a change of the density of diffusive states. This theoretical work also confirms the experimental result– no weak localization in graphene [61]. Y. W. Tan *et al.* [49] are experimentally investigated the  $\sigma_{min}$  vary in the range of  $2-12e^2/h$  for different graphene samples with various levels of disorder and mobility in the range of  $1-20 \times 10^3 \text{ cm}^2/\text{V s}$ , which can be related to the residual density induced by the inhomogeneous charge distribution in the samples.

In recent papers several authors applied the Landauer formula, instead of Kubo formula, to determine  $\sigma_{min} = 4e^2/(\pi h)$  for a rectangular MLG system with aspect ratio  $W/L \ll 1$  [58, 59]. Similar formula used in BLG to determine  $\sigma_{min}$  where the coefficient  $1/2$ , instead of  $1/\pi$  in MLG [59].

Away from the Dirac point, S. V. Morozov *et al.* [42] experimentally demonstrated conductivity of both MLG and BLG depends on the gate voltage ( $V_g$ ) (or consequently on charge carrier) in some circumstances roughly as  $\sigma(E_f) \propto V_g$ . They found that conductivity of BLG rapidly increases with temperature at the Dirac point but, away from Dirac point, no changes are observed. Comparison of MLG and BLG conductivity clearly show that temperature dependent scattering in BLG is substantially weaker than in MLG.

The linear dependence of conductivity on carrier density in graphene can be explained theoretically in the framework of Boltzmann transport theory by assuming Coulomb scatterers [30, 55, 62-64] rather than the short range scatterers. Hwang, Adam and Sharma [62] shows the graphene conductivity calculated including both charge impurity ( $n_i$ ) and short-range neutral impurity ( $n_p$ ) for different values of  $n_p/n_i$ . For small  $n_p/n_i$  (i.e  $\ll 1$ ), the conductivity is linear in density, which is seen in most experiments, and for large  $n_p/n_i$  ( $\sim 0.2$ ) the total conductivity shows the sublinear behavior which is also found in experiments [41, 49] for very high-mobility samples where short-range disorder plays a more dominant role.

Theoretically temperature-dependent conductivity of MLG [31] and BLG [33, 54, 65, 66] due to screened Coulomb disorder is calculate in past. Hwang and Sarma [31] show that temperature dependence of conductivity is exponentially suppressed as the temperature increases and shows typical metallic temperature dependence in the low temperature limit, but the high-temperature limit ( $T \rightarrow \infty$ ) of the conductivity increases as the temperature

increases, shows insulating system, and approaches half of the conductivity calculated at low-temperature limit ( $T \rightarrow 0$ ). These results also confirmed by recent experiments [67-70].

S. D. Sarma, E. H. Hwang and E. Rossi [54] show that temperature dependence conductivity of BLG is very weak at high densities and strong insulating-type  $T$  dependence at low densities as observed in recent experiments [42]. At low temperatures ( $T/T_f \ll 1$ ) the conductivity decreases linearly with temperature and shows the metallic behavior as explained with screened Coulomb impurities, but conductivity increases quadratically in high-temperature limit. By contrast, for the short-range disorder conductivity always increases with temperature. Similar result also found in Ref. [33]. More accurately, temperature dependent conductivity calculated at the Dirac point using the different approach- effective medium theory (EMT) [54]. At high density, the theory gives the same results as that obtained from the Boltzmann theory in the homogeneous case but at low densities (or at the Dirac point) there are significant deviations and give finite  $\sigma_{min}(T)$  due to the formation of inhomogeneous electron-hole puddles as experimentally observed.

## 1.4 Plasmons and Electron Energy Loss Function

### 1.4.1 Plasmons: Graphene and Nobel Metals

Plasmons are simply defined as collective oscillations of the electron in conduction band. Normally in bulk material plasmons are generated in two different regions: bulk region (i.e. bulk plasmons) and surface region (i.e. surface plasmons). Bulk plasmons are longitudinal oscillations of free electrons within the bulk of a material while surface plasmons (SPs) are coherent delocalized electron oscillation at the interface between material and dielectric. SPs in graphene can be coupled with photons, electrons or phonons. It will form SPPs (Surface Plasmon Polaritons) with photons, and composite “plasmaron” particles

with electrons. Plasmons or SPPs\* (\*Plasmons and SPPs are same in graphene because electrons in graphene are essentially frozen in the transverse dimension) excited in graphene are confined much more strongly than those in conventional noble metals. Here are some interesting properties of graphene, which makes it best plasmonics material as compared to the noble metal plasmonic materials;

### **(1) Extremely high confinement**

The wavelength of graphene SPPs is much smaller than the wavelength of metal SPPs, which results in a larger degree of confinement. The confinement of SPPs, which describes the ability of confining light, is generally valued by the vertical decay length (i.e. penetration depth). Simulation results showed that the vertical decay length of SPPs decreases with increasing of doping concentration in graphene [71-73] which is much higher than that of metals and it will be more helpful for applications in subwavelength optics.

### **(2) Relatively low loss in THz and infrared frequencies**

Conventional metals (like Au, Ag) are the ideal plasmonic materials in visible and near-infrared frequencies due to low loss in this range. The loss of metal plasmonic materials will increase dramatically with the decrease of frequency owing to the increased imaginary part of dielectric constants. Graphene does not have this kind of problem in THz due to smaller imaginary part of dielectric constant and penetration depth in THz as compared to noble metals [74].

### **(3) High tunability**

The tunability of SPPs in graphene is the most attractive advantage other than metals, where plasmon cannot be tuned once the structure is fixed, in the point of view of optoelectronic device applications. SPPs in graphene can be tuned by different ways like - electrical and

chemical doping, epitaxial grow on different substrates [75], changing the magnetic field and temperatures [76]. The working frequencies of graphene SPs are in THz and infrared regions, and if such frequencies can be extended to near-infrared or even visible regions through the composition of graphene with metal with high tunability [77, 78].

#### (4) Long relaxation time of electrons

The relatively large conductivity of graphene translates into long optical relaxation times reaching values of  $\tau = 10^{-13}$  s, compared to  $10^{-14}$  s in gold, thus providing a plausible solution to the long-standing problem of dissipation in plasmonics [79-81].

The dispersion relation of SPs is very important for graphene plasmonics, and numerous achievements have been made both in theory and experiment, such as Semi-classical model [82], Random-phase approximation (RPA) [25, 26, 83], tight-binding approximation [84], first-principle calculation [85], Dirac equation continuum model [86] and electron energy loss spectroscopy (EELS) experiments [87] etc. Among them, the Semi-classical model and RPA are commonly used in theoretical analysis, and EELS is very prevalent for experimental study. In RPA, plasmon dispersion relation can be defined by the poles of density-density response function,  $\Pi(q, \omega)$  or equivalently, from the zeroes of dynamical dielectric function,  $\epsilon(q, \omega)$ :

$$\epsilon(q, \omega_p - i\eta) = 0, \tag{1.47}$$

where,  $\omega_p$  is the plasmon frequency at a given wave vector  $q$  and  $\eta$  is the Landau damping rate (i.e. plasmons can decay by exciting an electron-hole pair) of plasma oscillations. In  $\omega$  complex plane, if the poles of  $\Pi(q, \omega)$  are on the real axis then the plasmons are long-lived and well-defined. However if the poles are away from real axis, we have the Landau damped plasmons due to the electron scattering. In the case of weak damping ( $\eta \ll \omega_p$ ), which is

more closer to the real situation, the imaginary part is negligibly small and thus, the plasmon dispersion is given by:

$$\text{Re}[\epsilon(q, \omega_p)] = 0. \quad (1.48)$$

Electron energy loss function (EELF) is an important quantity which is directly measured in spectroscopic techniques like high resolution electron energy loss spectroscopy (EELS). This quantity is proportional to the imaginary part of inverse dielectric function,  $\text{Im}[1/\epsilon(q, \omega)]$ .

### 1.4.2 Recent Works on Plasmons and Electron Energy Loss Function

Since the discovery of graphene, there have appeared a large number of research papers and also a number of review articles on graphene [14, 38, 39, 88]. The last decade has witnessed a spectacular surge in the number of publications dealing with surface plasmons (SPs) [88]. SPs has been experimentally demonstrated using different techniques, such as terahertz [89] and IR [90] optical spectroscopies. These experiment results confirm that graphene has emerged as one of the most promising research materials in the field of plasmonics.

M. Jablan *et. al* [83] have studied plasmons and their losses in doped graphene using RPA with relaxation-time approximation from experimentally available input parameters, and theoretical estimates for the relaxation- time utilizing electron-phonon coupling. They show that for sufficiently large doping values high wave localization and low losses are simultaneously possible for frequencies below that of the optical phonon branch  $\omega < \omega_{oph}$  (i.e.,  $E_{plasmon} < 0.2 \text{ eV}$ ).

J. Yan *et. al* [85] investigated the role of substrates on the collective excitations of graphene by using a first-principles implementation of the density response function within RPA. First-principles calculations show that the plasmons in graphene are significantly

damped by a semiconducting substrate and completely quenched by a metallic substrate, in particular, in the long wavelength limit. The electronic response is dominated by the long ranged Coulomb interaction which makes the effect significant even for weakly coupled graphene-substrate systems.

E. Hwang and S. D. Sarma [25] and B. Wunsch *et al.* [26] had tried to deal with doped graphene by RPA at zero temperature under self-consistent-field linear response theory. In the long-wavelength limit ( $q \rightarrow 0$ ), the dispersion of SPs mode for a MLG can be expressed as  $\omega_{sp}(q \rightarrow 0) \propto n_c^{1/4} \sqrt{q}$ , which is different from the other 2D parabolic band materials where  $\omega_{sp}(q \rightarrow 0) \propto n_c^{1/2} \sqrt{q}$ . For finite value of  $q$ , the parabolic trend of dispersion relation disappears. The dispersion relation of graphene SPs can also be studied by EELS experiments [87]. Later, M. R. Ramezani *et al.* [32] and Z. Z. Li [91] have studied the Coulomb screening and plasmon dispersion of doped MLG at finite temperatures in the RPA.

The electromagnetic response of graphene and the spectrum of collective plasmon excitations are studied using the tight-binding approximation, including both valleys, by A. Hill, S.A. Mikhailov and K. Ziegler [84]. Their results agree with those experiments for low energies in Ref. [92], whereas the high-energy results of Ref. [93] are beyond tight-binding approximation. Furthermore, inter-valley plasmons in graphene have been studied in the tight-binding approximation by T. Tudorovskiy & S. A. Mikhailov [94], relating them to transitions between the two nearest Dirac cones.

Some recent experiments on graphene's plasmons [93, 95, 96] show that plasmon frequency ( $\omega_p$ ) at long wavelength is linear function of  $q$  (in contrast to  $\omega_p \propto \sqrt{q}$ ), which is thought to be due to many-body interactions and the local-field effect [94, 95].

S. A. Mikhailov and K. Ziegler [97] recently found a new transverse electric (TE) mode in graphene, which cannot exist in systems with the parabolic electron dispersion, in the terahertz range (THz),  $1.667 < \hbar\omega/E_f < 2$  or  $15 \text{ THz} < f(\text{frequency}) < 18 \text{ THz}$  and it can be tuned from the radio-frequency range to the infrared by changing the density of charge carriers using a gate voltage.

P. K. Pyatkovskiy [27] assumed an unspecified energy gap of arbitrary width for doped MLG and studied the corresponding dynamically screening and plasmons at zero temperature in RPA. Furthermore, a THz source has been proposed based on the stimulated plasmon emission in graphene [98] and the absorption of THz electromagnetic radiation in gapped graphene has been estimated [99]. X. F. Wang and T. Chakraborty [100] have studied the effect of finite energy gap due to spin orbital interaction (SOI) on plasmons dispersion of undoped and doped MLG at finite temperatures in the RPA.

The collective excitations in zero gap BLG have been studied in previous work at zero-temperature [101] and finite temperatures [102] within two-band parabolic single-particle band-dispersion approximation. The long-wavelength BLG plasmon is identical to the ordinary 2D plasmon and is different from the long-wavelength MLG plasmon. The parabolic band-structure approximation would fail at high energy where the BLG single-particle dispersion becomes linear, similar to MLG and hyperbolic dispersion is relevant at high energies. Later, X. F. Wang and T. Chakraborty [103] have studied the effect of the potential bias on collective excitations of gapped BLG at both zero and finite temperature. The potential bias opens a gap in the single-particle excitation spectrum and softens the collective excitation modes. This may result in undamped collective excitation modes that are observable in experiments. In the single gate configuration, the doping and gate voltage can vary the potential bias and the carrier density of the BLG and manipulate the energy and

lifetime of the collective excitation modes inside. Intriguing situations with potential application are systematically explored and discussed by W. L. You and X. F. Wang [104] on external controlling factors such as perpendicular electric bias, temperature, doping, and substrate background provides great freedom to manipulate the low-energy plasmon dispersion of the BLG. They also found extra undamped plasmon modes appear at energies close to the band gap energy under electric bias and have almost zero group velocities.

Some papers have reported the collective excitation spectrum using the full 4-band continuum model within the RPA instead of the simplified 2-band model for both gapless [28, 105] and gapped BLG [106]. The dielectric screening function and the plasmon modes have a qualitatively different character in the 4-band model compared to the ones obtained using the simplified 2-band model, especially when gap is not zero.

## 1.5 Objectives of Thesis

Apart from promising applications for technological innovations, Graphene offers a new and novel physics. Properties of Graphene sharply differ from that of 2DEG observed in doped semiconductor heterostructures. One of the important properties that is a requisite for device making is charge transport. Theoretical studies suggest that by consideration of a scattering mechanism based on screened charged impurities; one can obtain conductivity from a Boltzmann equation approach that agrees with the experimental result on Graphene. But most of the calculated analytical and numerical expressions of MLG and BLG are restricted to the case of zero temperature whereas the experimental study of electrical conductivity is carried out at a finite temperature. Also, the specific and detailed results on the effects of finite temperature and energy gap on the plasmons and Electron Energy Loss Function in MLG have not been carried out. Thus the two main objectives of this research are;

(1) to study screened electronic transport properties of MLG and BLG as a function of intrinsic parameters like quasi particle energy, temperature, impurity concentration, and energy gap within the Boltzmann Transport Equation,

(2) to study the finite temperature effects on non-interacting dynamical polarization function, plasmon modes, and electron energy loss function of doped MLGG within the random phase approximation.

I believe that the results presented in this work will be helpful in understanding whole new class of graphene based nanoelectronic and optoelectronic devices.

## 1.6 References

- [1] R. E. Peierls, Ann. I. H. Poincare **5**, 177 (1935).
- [2] L. D. Landau, Phys. Z. Sowjetunion **11**, 26 (1937).
- [3] P. R. Wallace, Phys. Rev. **71**, 622 (1947).
- [4] J. W. McClure, Phys. Rev. **104**, 666 (1956).
- [5] J. C. Slonczewski and P. R. Weiss, Phys. Rev. **109**, 272 (1958).
- [6] E. Fradkin, Phys. Rev. B **33**, 3263 (1986).
- [7] K. S. Novoselov *et al.*, Science **306**, 666 (2004).
- [8] Y. Zhang *et al.*, Nature London **438**, 201 (2005).
- [9] I. Vlassiouk *et al.*, ACS Nano. **5**, 6069 (2011).
- [10] M. Ishigami *et al.*, Nano Letters. **7**, 1643 (2007).
- [11] Y. Hernandez *et al.*, Nat Nano. **3**, 563 (2008).
- [12] D. P. DiVincenzo and E. J. Mele, Phys. Rev. **295**, 1685 (1984).
- [13] A. K. Geim and K. S. Novoselov, Nat. Mater. **6**, 183 (2007).
- [14] A. H. Castro Neto *et al.*, Rev. Mod. Phys. **81**, 109 (2009).
- [15] C. Lee, X. Wei and J. Hone, Science **321**, 385 (2008).
- [16] J. S. Bunch *et al.*, Nano Letters **8**, 2458 (2008).
- [17] T. Enoki and T. Ando (Editor), *“Physics and Chemistry of Graphene: Graphene to Nanographene”*, Pan Stanford Publishing (2013).
- [18] M. Koshino, New J. Phys. **11**, 095010 (2009).
- [19] I. Gierz *et al.*, Nano Lett. **8**, 4603 (2008).

- [20] D. A. Siegel *et al.*, Appl. Phys. Lett. **93**, 243119 (2008).
- [21] S. Y. Zhou *et al.*, Physica E **40**, 2642 (2008).
- [22] G. Giovannetti *et al.*, Phys. Rev. B **76**, 073103 (2007).
- [23] S. D. Sarma, E. H. Hwang and W. K. Tse, Phys. Rev. B **75**, 121406 (2007).
- [24] M. I. Katsnelson, Phys. Rev. B **74**, 201401(R) (2006).
- [25] E. H. Hwang, S. D. Sarma, Phys. Rev. B **75**, 205418 (2007).
- [26] B. Wunsch *et al.*, New J. Phys. **8**, 318 (2006).
- [27] P. K. Pyatkovskiy, J. Phys.: Condens. Matter **21**, 025506 (2009).
- [28] O. V. Gamayun, Phys. Rev. B **84**, 085112 (2011).
- [29] J. N. Zhang, Phys. Scr. **83**, 035002 (2011).
- [30] T. Ando, J. Phys. Soc. Jpn. **75**, 074716 (2006).
- [31] E. H. Hwang, and S. D. Sarma, Phys. Rev. B **79**, 165404 (2009).
- [32] M. R. Ramezanali *et al.*, J. Phys. A: Math. Theor. **42** 214015 (2009).
- [33] M. Lv and S. Wan, Phys. Rev. B **81**, 195409 (2010).
- [34] N. W. Ashcroft and N. D. Mermin, "*Solid State Physics*", Thomson Learning, Toronto (1976).
- [35] R. A. Jishi, "*Feynman Diagram Techniques in Condensed Matter Physics*", Cambridge University Press (2013).
- [36] T Ando *et. al.*, (2002).
- [37] M. Muller, J. Schmalian and L. Fritz, Phys. Rev. Lett. **103**, 025301 (2009).
- [38] N. M. R. Peres, Rev. Mod. Phys. **82**, 2673 (2010).

- [39] S. D. Sarma *et al.*, Rev. Mod. Phys. **83**, 407 (2011).
- [40] K. S. Novoselov *et al.*, Nature **438**, 197 (2005).
- [41] J. H. Chen *et al.*, Nat. Phys. **4**, 377 (2008).
- [42] S. V. Morozov *et al.*, Phys. Rev. Lett. **100**, 016602 (2008).
- [43] K. S. Novoselov *et al.*, Nature Phys. **2**, 177 (2006).
- [44] R. V. Gorbachev *et al.*, Phys. Rev. Lett. **98**, 176805 (2007).
- [45] B. E. Feldman, J. Martin and A. Yacoby, Nat. Phys. **5**, 889 (2009).
- [46] K. Ziegler, Phys. Rev. B **75**, 233407 (2007).
- [47] B. Dóra, K. Ziegler and P. Thalmeier, Phys. Rev. B **77**, 115422 (2008).
- [48] C. Jang *et al.*, Phys. Rev. Lett. **101**, 146805 (2008).
- [49] Y. W. Tan *et al.*, Phys. Rev. Lett. **99**, 246803 (2007).
- [50] N. H. Shon and T. Ando, J. Phys. Soc. Jpn. **67**, 2421 (1998).
- [51] M. Koshino and T. Ando, Phys. Rev. B **73**, 245403 (2006).
- [52] T. Fukuzawa, M. Koshino and T. Ando, J. Phys. Soc. Jpn. **78**, 094714 (2009).
- [53] E. Rossi, S. Adam and S. D. Sarma, Phys. Rev. B **79**, 245423 (2009).
- [54] S. D. Sarma, E. H. Hwang and E. Rossi, Phys. Rev. B **81**, 161407 (2010).
- [55] K. Ziegler, Phys. Rev. Lett. **97**, 266802 (2006).
- [56] K. Nomura and A. H. MacDonald, Phys. Rev. Lett. **98**, 076602 (2007).
- [57] J. Cserti, Phys. Rev. B **75**, 033405 (2007).
- [58] J. Tworzydło *et al.*, Phys. Rev. Lett. **96**, 246802 (2006).
- [59] M. I. Katsnelson, Eur. Phys. J. B **51**, 157 (2006).

- [60] I. Snyman and C. W. J. Beenakker, Phys. Rev. B **75**, 045322 (2007).
- [61] S. V. Morozov *et al.*, Phys. Rev. Lett. **97**, 016801 (2006).
- [62] E. H. Hwang, S. Adam and S. Das Sarma, Phys. Rev. Lett. **98**, 186806 (2007).
- [63] S. Adam and S. D. Sarma, Phys. Rev. B **77**, 115436 (2008).
- [64] M. Trushin and J. Schliemann, Europhys. Lett. **83**, 17001 (2008).
- [65] S. Adam and M. D. Stiles, Phys. Rev. B **82**, 075423 (2010).
- [66] E. H. Hwang and S. D. Sarma, Phys. Rev. B **82**, 081409 (2010).
- [67] Y. W. Tan *et al.*, Eur. Phys. J. Special Topics **148**, 15 (2007).
- [68] K. I. Bolotin *et al.*, Phys. Rev. Lett. **101**, 096802 (2008).
- [69] J. H. Chen *et al.*, Nature Nanotech. **3**, 206 (2008).
- [70] W. Zhu *et al.*, Phys. Rev. B **80**, 235402 (2009).
- [71] A. Vakil and N. Engheta, Science **332**, 1291 (2011).
- [72] Z. Fei *et al.*, Nature **487**, 82 (2012).
- [73] J. Chen *et al.*, Nature **487**, 77 (2012).
- [74] W. B. Lu *et al.*, Opt. Express **21**, 10475 (2013).
- [75] L. Wang *et al.*, Opt. Lett. **37**, 2730 (2012).
- [76] J. Y. Wu *et al.*, ACS Nano **5**, 1026 (2011).
- [77] J. Kim *et al.*, Nano Lett. **12**, 5598 (2012).
- [78] N. K. Emani *et al.*, Nano Lett. **12**, 5202 (2012).
- [79] J. Christensen *et al.*, ACS Nano **6**, 431 (2012).
- [80] J. M. Dawlaty *et al.*, Appl. Phys. Lett. **92**, 042116 (2008).

- [81] P. Neugebauer *et al.*, Phys. Rev. Lett. **103**, 136403 (2009).
- [82] G. W. Hanson, J. Appl. Phys. **103**, 064302 (2008).
- [83] M. Jablan, H. Buljan and M. Soljac'ic', Phys. Rev. B **80**, 245435 (2009).
- [84] A. Hill, S. A. Mikhailov and K. Ziegler, Europhys. Lett. **87**, 27005 (2009).
- [85] J. Yan, K. S. Thygesen and K. W. Jacobsen, Phys. Rev. Lett. **106**, 146803 (2011).
- [86] M. Bordag and I. G. Pirozhenko, Phys. Rev. B **89**, 035421 (2014).
- [87] S. Y. Shin *et al.*, Appl. Phys. Lett. **99**, 082110 (2011).
- [88] X. Luo *et al.*, Mater. Sci. Eng. R **74**, 351 (2013).
- [89] L. Ju *et al.*, Nat. Nanotech. **6**, 630 (2011).
- [90] Z. Fei *et al.*, Nano Lett. **11**, 4701 (2011).
- [91] Z. Z. LI, Commun. Theor. Phys. **52**, 361 (2009).
- [92] Liu Yu *et al.*, Phys. Rev. B. **78**, 201403(R) (2008).
- [93] T. Eberlein *et al.*, Phys. Rev. B **77**, 233406 (2008).
- [94] T. Tudorovskiy and S. A. Mikhailov, Phys. Rev. B. **82**, 073411 (2010).
- [95] C. Kramberger *et al.*, Phys. Rev. Lett. **100**, 196803 (2008).
- [96] J. Lu *et al.*, Phys. Rev. B **80**, 113410 (2009).
- [97] S. A. Mikhailov and K. Ziegler, Phys. Rev. Lett. **99**, 016803 (2007).
- [98] F. Rana, IEEE Trans. Nanotechnol. **7**, 91 (2008).
- [99] A. R. Wright *et al.*, Microelectron. J. **40**, 857 (2009).
- [100] X. F. Wang and T. Chakraborty, Phys. Rev. B **75**, 033408 (2007).

- [101] R. Sensarma, E. H. Hwang and S. D. Sarma, Phys. Rev. B. **82**, 19542 (2010).
- [102] X. F. Wang and T. Chakraborty, Phys. Rev. B **75**, 041404 (2007).
- [103] X. F. Wang and T. Chakraborty, Phys. Rev. B **81**, 081402 (R) (2010).
- [104] W. L. You and X. F. Wang, Nanotechnology **23**, 505204 (2012).
- [105] G. Borghi *et al.*, Phys. Rev. B **80**, 241402 (R) (2009).
- [106] C. Triola and E. Rossi, Phys. Rev. B **86**, 161408(R) (2012).